Resources Chemicals and Materials xxx (xxxx) xxx

Contents lists available at ScienceDirect

Resources Chemicals and Materials

journal homepage: www.keaipublishing.com/en/journals/resources-chemicals-and-materials/

Efficient corn stover-derived metal-supported biochar catalyst for hydrogenation of xylose to xylitol

Kridsada Karin [a,b], Sanchai Kuboon [c], Bunyarit Panyapinyopol [a,b], Saran Youngjan [c], Wanwitoo Wanmolee [d,e], Nawin Viriya-empikul [f], Navadol Laosiripojana [f], Kamonwat Nakason [a,b,*]

[a] Department of Sanitary Engineering, Faculty of Public Health, Mahidol University, Bangkok, Thailand
[b] Center of Excellence on Environmental Health and Toxicology (EHT), OPS, MHESI, Bangkok, Thailand
[c] National Nanotechnology Center (NANOTEC), National Science and Technology Development Agency (NSTDA), Pathumthani, Thailand
[d] Department of Chemical Engineering, Faculty of Engineering, King Mongkut's University of Technology North Bangkok (KMUTNB), Bangkok, 10800, Thailand
[e] Center of Eco-Materials and Cleaner Technology, King Mongkut's University of Technology North Bangkok, Bangkok 10800, Thailand
[f] The Joint Graduate School of Energy and Environment, King Mongkut's University of Technology Thonburi, Bangkok, Thailand

ARTICLE INFO

Keywords:
Xylitol
Platform chemical
Hydrogenation reaction
Heterogeneous catalyst
Waste utilization
Bimetallic catalyst

ABSTRACT

Xylitol, one of the top twelve chemical building blocks, is commercially synthesized through the xylose hydrogenation reaction using a metal catalyst. Biochar has emerged as an eco-efficient catalyst support material. In this study, biochar derived from corn stover (BCS) was first used as a metal catalyst support material for xylose hydrogenation into xylitol. The catalyst was prepared by carbonizing corn stover (CS), impregnating the resulting biochar with metal, and reducing the metal-impregnated BCS. The catalyst characteristics were comprehensively explored. The Ru/BCS catalyst was employed in xylose conversion to xylitol at different process temperatures (100 – 160 °C), retention times (3 – 12 h), H_2 pressures (2 – 5 MPa), and Ru contents (1 – 5 %). The highest xylitol yield (87.0 wt.%) and selectivity (91.6 %) were derived at 120 °C for 6 h under 4 MPa H_2 using 5 % Ru. Interestingly, the Ru/BCS catalyst showed high stability under the promising process condition. Additionally, xylitol production from hydrolysates enriched with CS xylose was subsequently explored. On the other hand, the catalyst characterization results revealed that the superior catalytic efficiency of 5Ru/BCS was mainly due to the metal nanoparticles embedded in the biochar. Additionally, BCS proved to be an outstanding support material for a bimetallic hydrogenation catalyst (Ru-Ni/BCS). Therefore, these results indicate that BCS can be a competitive support material for metal hydrogenation catalysts, enhancing environmental friendliness and potentially being employed in industrial-scale xylitol production.

1. Introduction

The production of valuable chemicals and biofuels from lignocellulosic biomass represents a cornerstone of sustainable development and the transition to a bio-based economy [1-3]. Xylitol, identified as one of the top twelve dominant chemical building blocks, is produced from xylose, a monosaccharide found in the hemicellulose component of biomass [4,5]. Xylitol, a pentitol with extensive applications in the food, pharmaceutical, nutraceutical, cosmetic, beverage, and dental care industries, is valued for its high-water solubility, sweetening power, low-calorie content, low glycemic index, non-interference with food nutritional value, anticariogenic properties, prevention of ear infections, near insulin-independent metabolism, and ability to re-harden teeth [6-8]. Additionally, xylitol can be used as a building block chemical in various industries, including biofuels, textiles, furniture, and polymers [4].

Industrial xylitol production is conventionally performed through the xylose hydrogenation process using a Raney nickel (Ra-Ni) catalyst [9]. The Ra-Ni catalyst has several major advantages, including its low cost, ease of use as a suspended slurry in batch processes, and outstanding catalytic activity [10,11]. However, its principal limitations are relatively fast deactivation and metal leaching [12-14]. Recently, various noble metals (Ru, Pt, and Pd) supported on conventional substrates have been demonstrated in xylitol production, with Ru-based

* Corresponding author.
E-mail address: kamonwat.nak@mahidol.ac.th (K. Nakason).

https://doi.org/10.1016/j.recm.2024.10.002
Received 9 July 2024; Received in revised form 28 September 2024; Accepted 9 October 2024
Available online 19 October 2024

catalysts showing a low deactivation rate and excellent selectivity [14,15]. Interestingly, several research works have explored different materials supporting Ru catalysts with high catalytic activity and selectivity, such as TiO_2 [15], NiO-modified TiO_2 [16], and zeolite [17]. However, metal- and zeolite- supported Ru catalysts exhibit some limitations, including raw material availability and sustainability, catalyst production and disposal, and metal-support interaction. Typically, the metal- supported Ru catalysts use non-renewable materials as supports. The production and sourcing of these materials have significant environmental impacts, including energy-intensive extraction processes, mining, and refining, which contribute to greenhouse gas emissions and habitat destruction. Zeolite-supported Ru catalysts are microporous aluminosilicate materials, synthesized or mined naturally. Natural zeolite mining has environmental consequences like land degradation and dust emissions. When metal- and zeolite- supported Ru catalysts deactivated, these catalysts can generate toxic waste, disposing of spent metal-supported catalysts poses environmental concerns due to heavy metal contamination and the difficulty in recovering Ru. Additionally, the metal-supported Ru catalysts can interact weakly with Ru, leading to poor dispersion and uneven distribution of Ru nanoparticles, and the zeolite-supported Ru catalysts provide high surface areas, the small pore sizes can restrict access to active Ru sites, particularly for larger reactant molecules. This reduces the overall effectiveness of the catalyst for reactions involving bulky molecules. Therefore, to overcome these limitations, developing efficient, cost-effective, and environmentally friendly materials supporting Ru catalysts remains a significant challenge. Recent advancements in biochar, a carbon-rich material obtained from renewable biomass carbonization, have demonstrated its potential as a sustainable catalyst support due to the richness of functional groups (-OH, C=O, and -COOH) [18,19]. These functional groups are more favorable for surface functionalization and anchoring metal nanoparticles [20]. The C=O and -COOH groups on the biochar surface provide ideal nucleation sites for noble metal nanoparticles, which can substantially enhance the dispersion and stability of metal nanoparticles [20]. Biochar from various biomass sources, including fir sawdust [21], beetroot [22], coconut shell [23,24], microcrystalline cellulose [25], and cassava dregs [26] was modified and employed as metal catalyst supporting material in hydrogenation reactions for the producing 4-nitrophenol, aniline, phenol, 2,5-dimethylfuran, and sorbitol, respectively. Interestingly, to the best of our knowledge, the use of conventional biochar (unmodified biochar) as a metal catalyst supporting material in hydrogenation reactions for xylitol production has never been explored.

Corn stover (CS), the residual biomass remaining after corn harvest, is an abundant and underutilized agricultural byproduct [27]. In 2022, the global corn product reached 1137 million tons, with a residue product ratio of 2.08 [28,29]. Thus, the estimated quantity of corn stover (CS) is around 2365 million tons. Typically, after corn is harvested, CS is disposed of through field burning, which contributes to significant environmental pollution, particularly global warming. Addressing this issue requires the development of effective methods to repurpose CS for high-value products. Being rich in cellulose, hemicellulose, and lignin, the substantial lignocellulosic compositions of CS suggest its potential use as a catalyst support via carbonization [26,30,31]. Interestingly, the application of biochar produced from CS carbonization as a catalyst support specifically for xylitol production remains unexplored.

In this study, CS biochar was employed as a support for single- and bi-metallic hydrogenation catalysts, and CS xylose was extracted for xylitol production. This research purposed to explore the potential of xylose conversion into xylitol over the CS-derived metal-supported biochar catalyst and to observe the properties of this catalyst. Additionally, the influences of process temperature, retention time, hydrogen pressure, and metal content on xylitol production were investigated. Xylitol production from hydrolysate-enriched CS xylose was further evaluated in separate one-pot catalytic reactions.

2. Materials and methods

2.1. Catalyst preparation and characterization

Corn stover (CS) with 10.25 wt.% moisture content was collected from a corn plantation in Tha Wang Pha District, Nan Province, Thailand. It was chopped, cleaned, sun-dried, pulverized, and electrically dried to obtain dried CS powder with a particle size ranging from 150 to 600 μm [18,32]. The obtained CS powder was preserved in a sealed sample collection bag before subsequent investigation. $RuCl_3{\cdot}3H_2O$ and Ru/C was commercially obtained from Sigma-Aldrich, Canada. $Ni(NO_3)_2{\cdot}6H_2O$ was purchased from Qrec Co. Ltd., New Zealand.

A metal-supported biochar catalyst was prepared through carbonization, impregnation, drying, and reduction. Carbonization of the CS (3 g) was performed at 500 °C for 1 h under 100 mL/min CO_2 to achieve the biochar CS (BCS). Impregnation of the BCS was subsequently conducted at room temperature for 4 h under a continuous stirring rate of 200 rpm. In each impregnation, 1 g BCS was homogeneously blended with $RuCl_3{\cdot}3H_2O$ and $Ni(NO_3)_2{\cdot}6H_2O$, and 80 mL ultra-pure water to obtain 1 %Ru/BCS (1Ru/BCS), 3 %Ru/BCS (3Ru/BCS), 5 %Ru/BCS (5Ru/BCS), 3 %Ru-1 %Ni/BCS (3Ru-1Ni/BCS), 3 %Ru-2 %Ni/BCS (3Ru-2Ni/BCS), 2 %Ru-3 %Ni/BCS (2Ru-3Ni/BCS), and 5 %Ni/BCS (5Ni/BCS) catalysts. Afterwards, the impregnated BCS was segregated from the liquid phase, dried, and reduced through the similar steps demonstrated in the previous work [31]. Briefly, during the reduction step, the impregnated BCS was treated at 250 °C under a 100 mL/min N_2 flow for 3 h, followed by the same treatment conditions under a H_2 atmosphere for the reduction process. The obtained catalysts were stored in sample collection bottles under a nitrogen atmosphere for subsequent experiments.

The characteristics of the raw CS were examined in terms of proximate, ultimate, and lignocellulosic compositions. The lignocellulosic material, ash, moisture, and volatile matter (VM) contents were assessed using the methods outlined in NREL/TP-510–42618 [33], NREL/TP-510–42622 [34], ASTM E1756 [35], and ASTM D7582 [36], respectively. Fixed carbon (FC) content was calculated by deducting the combined ash and VM contents from 100 %. The elemental contents of carbon (C), hydrogen (H), nitrogen (N), and sulfur (S) were determined using an elemental analyzer (LECO CHNS 628, LECO, USA). Oxygen content was calculated from the remaining mass fraction, excluding ash.

The catalyst characteristics were explored through various analyses, including ultimate compositions, Ru and Ni contents, reducibility, interaction strength between metal and hydrogen, elemental chemical states, surface chemical functional groups, thermal decomposition properties, structural characteristics, nitrogen sorption properties, surface morphology, and structural morphology. The detailed methods of catalyst characterizations were elucidated in the Supplementary Materials [31].

2.2. Reaction and production analysis

Xylose was commercially supplied by Kemaus Co. Ltd., Australia. Hydrogenation of xylose to xylitol using the metal-supported biochar catalyst was performed in a 100 mL high pressure vessel (NK Laboratory Co., Ltd., Thailand). In each experimental setup, xylose (1 g), catalyst (0.25 g), and ultra-pure water (20 mL) were uniformly blended in the vessel, and the vessel was securely closed. H_2 gas at a specific pressure (2 – 5 MPa) at ambient temperature was then introduced into the vessel. Subsequently, the vessel was heated using an electrical furnace (Fig. 1) at temperatures ranging from 100 – 160 °C for 3 – 12 h with a stirring rate of 600 rpm. After the reaction, the vessel was rapidly cooled to room temperature. The liquid product was isolated from the spent catalyst by vacuum filtration. The obtained liquid product was preserved in an amber vial at 4 °C, and the spent catalyst was rinsed with deionized water, dried at 105 °C for 24 h, and preserved in a sample collection bottle for subsequent investigations. Each experiment was performed in

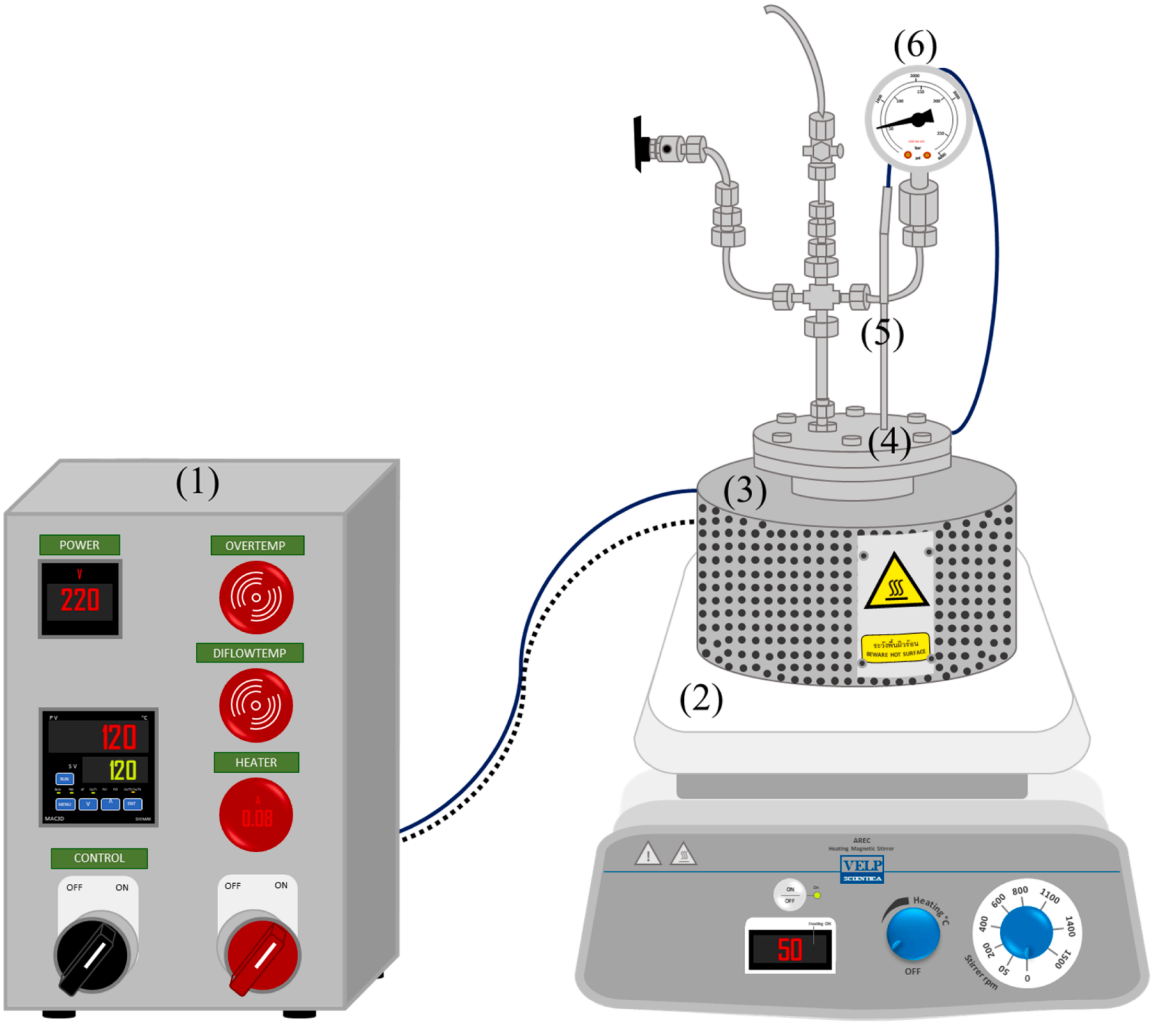

Fig. 1. Schematic diagram of equipment setup for xylitol production (1. Electrical controller, 2. Hot plate stirrer, 3. Electrical furnace, 4. Stainless steel reactor, 5. Thermocouple probe type K, and 6. Pressure gauge).

duplicate, and if discrepancies occurred (coefficient of variation greater than 10 %), a third trial was conducted to validate the results.

Xylose and xylitol contents in the liquid product were measured using high-performance liquid chromatography (HPLC Dionex Ultimate 3000, Thermo Scientific, USA) equipped with a refractive index detector (ERC RefractoMax 520, Thermo Scientific, USA) and a Shodex sugar SP0810 column. Degassed ultra-pure water was used as the mobile phase at a flow rate of 0.6 cm^3/min [37,38]. During the measurement, the column temperature was maintained at 80 °C for 20 min. Xylose and xylitol concentrations were determined using linear equations established by external calibration curves of standard solutions at various concentrations. Yield and selectivity of xylitol, and xylose conversion were quantified through Equations (1) – (3) [18,39]:

$$\text{Xylitol yield (wt.\%)} = \frac{\text{Xylitol weight (mg)}}{\text{Initial xylose weight (mg)}} \times 100\% \quad (1)$$

$$\text{Xylitol selectivity (\%)} = \frac{\text{xyliitol yield (wt.\%)}}{\text{Xylose conversion (wt.\%)}} \times 100\% \quad (2)$$

$$\text{Xylose conversion (wt.\%)} = \frac{\text{Initial xylose weight (g)} - \text{existed xylose weight (g)}}{\text{Initial xylose weight (g)}} \times 100\% \quad (3)$$

3. Results and discussion

3.1. Corn stover characteristics

Table 1 tabulates the pristine CS compositions. Proximate and ultimate components revealed that the pristine CS constituted lower fixed carbon (FC) and carbon contents than volatile matter (VM) and oxygen contents, respectively. This suggests that the devolatilization reactions during the carbonization process could produce CS biochar with

Table 1
The CS components.

Proximate analysis (wt.%)			Ultimate analysis (wt.%)					Lignocellulosic compositions (wt.%)		
Ash	VM	FC	C	H	N	S	O	Cellulose	Hemicellulose	Lignin
4.23	74.79	20.98	43.93	5.98	0.92	0.02	42.92	39.50	19.76	22.30

Table 2
Elemental compositions and textural properties of BCS, 5Ru/BCS, and 3Ru-2Ni/BCS.

Sample name	Elemental compositions (wt.%)							Textural properties		
	C	H	N	S	O	Ru	Ni	SSA (m^2/g)	Pore size (nm)	Pore volume (cm^3/g)
BCS	74.99	3.36	2.05	0.00	5.13	0.00	0.00	27.8	3.13	0.02
5Ru/BCS	73.49	3.14	1.52	0.00	12.39	0.06	0.00	21.1	3.13	0.02
3Ru-2Ni/BCS	64.98	2.12	1.45	0.00	13.14	0.42	1.41	35.5	3.51	0.03
Spent 5Ru/BCS	75.87	3.29	1.24	0.00	17.85	0.03	0.00	11.9	2.95	0.01

excellent properties for catalyst support [40,41]. Additionally, the high hemicellulose content in CS implies that it is feasible to extract CS xylose for xylitol production.

3.2. Catalyst characteristics

The elemental compositions of BCS, 5Ru/BCS, and 3Ru-2Ni/BCS are elucidated in Table 2. It can be observed that the BCS primarily consisted of carbon, with substantially lower oxygen and hydrogen levels compared to the pristine CS, owing to their removal during the carbonization process. This enhancement of the catalyst support properties of pristine CS was due to carbonization. However, some oxygen content remained in the BCS, identified as -OH, C=O, and -COOH groups, implying that the BCS surface could be an ideal nucleation site for noble metal nanoparticles [20]. The carbon proportion of 5Ru/BCS and 3Ru-2Ni/BCS catalysts was lower than that of the BCS, implying the appearance of metal elements on the BCS surface. Otherwise, the 5Ru/BCS and 3Ru-2Ni/BCS catalysts contained higher oxygen content than the BCS, likely due to the adsorption of oxygen on metal catalysts during elemental analysis [42]. The Ru content of the 5Ru/BCS was 0.06 wt.%, whereas the 3Ru-2Ni/BCS catalyst contained 0.42 wt.% Ru and 1.41 wt.% Ni, which were substantially lower than the theoretical value. Surprisingly, the Ru content of the 3Ru-2Ni/BCS catalyst was higher than that of the 5Ru/BCS, even though its addition content in the impregnation step was lower. This could be due to Ni enhancing the anchoring of Ru on the BCS. However, both Ru and Ni of 3Ru-2Ni/BCS reduced to 0.14 and 0.97 wt.%, respectively; and the Ru of the 5Ru/BCS catalyst diminished to 0.03 wt.% after use in the xylitol production process. These reductions were principally due to metal leaching during the xylose conversion process, which agrees with the appearance of Ru (0.05 mg/L) and Ni (0.24 mg/L) in the liquid product. On the other hand, the Ru leaching proportion of 3Ru-2Ni/BCS (66.7 %) was higher than that of 5Ru/BCS (50 %), suggesting that the BCS could be a promising alternative supporting material for a single metallic catalyst rather than a bimetallic catalyst.

The textural properties including specific surface area (SSA) and pore characteristics of BCS, 5Ru/BCS, and 3Ru-2Ni/BCS samples were determined by nitrogen adsorption isotherms with the BET and BJH methods. The samples demonstrated a type IV adsorption-desorption pattern featuring a type H4 hysteresis loop, according to IUPAC classification, across the range of P/P_0. The BCS, 5Ru/BCS, and 3Ru-2Ni/BCS samples had the SSAs of 27.8, 21.1, and 35.5 m^2/g, respectively (Fig. 2). Interestingly, SSA of the BCS was higher than that of cassava dregs biochar (10.5 m^2/g) [26], indicating that BCS could be a dominant catalyst supporting mesoporous material. On the other hand, the introduction of the metallic phases marginally changed the SSA, pore size, and pore volume of the BCS (Table 2). These changes were more noticeable with the introduction of Ni phase, implying that Ni

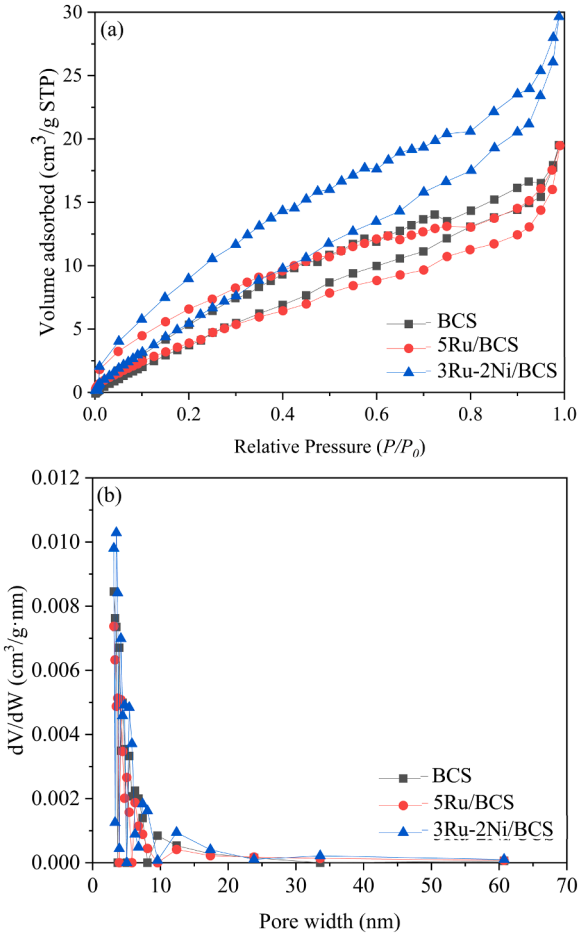

Fig. 2. (a) N_2 adsorption desorption isotherm and (b) pore size distribution of BCS, 5Ru/BCS, and 3Ru-2Ni/BCS.

nanoparticles were successfully introduced to the BCS. Similar trends of textural property changes were reported in carbon supported Ru-Ni bimetallic catalyst [43].

To understand the H_2 consumption behaviors of the catalyst, the reducibility of 5Ru/BCS and 3Ru-2Ni/BCS catalysts was assessed using temperature-programmed reduction of hydrogen (H_2-TPR), as depicted in Fig. 3(a). The TPR profiles of the 5Ru/BCS catalyst demonstrate two ranges of hydrogen consumption at low (100 – 220 °C) and high (230 – 460 °C) temperatures. The reduction at low temperature is associated with the electron-deficient ruthenium species converting to metallic

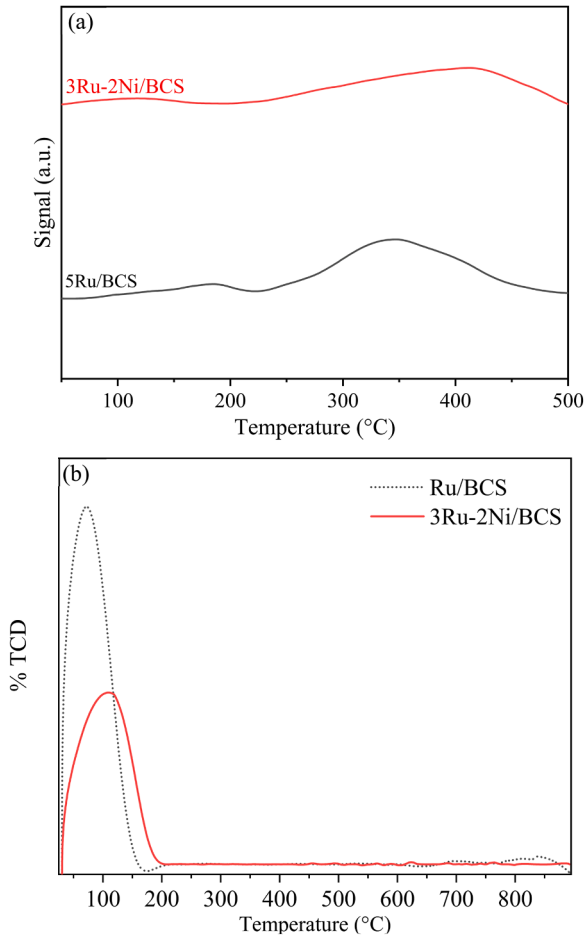

Fig. 3. (a) H_2-TPR and (b) H_2-TPD profiles of 5Ru/BCS and 3Ru-2Ni/BCS catalysts.

ruthenium, suggesting the presence of $RuCl_3$ and RuO_2 species in the catalyst obtained via wet impregnation of $RuCl_3$ [44]. Furthermore, the reduction temperature of ruthenium chloride is lower than that of ruthenium oxide [45,46], and the decrease in chlorine content in ruthenium catalysts contributes to metal oxide formation, shifting the reduction to higher temperatures [47]. Therefore, the $RuCl_3$ reduction corresponds to the H_2 consumption peak at low temperature, while the RuO_2 reduction is associated with the high-temperature peak. Similarly, the TPR profiles of the 3Ru-2Ni/BCS catalyst display two ranges of hydrogen consumption at low (50 – 175 °C) and high (300 – 500 °C) temperatures. The hydrogen consumption at low temperature aligns with the $RuCl_3$ reduction. The second hydrogen consumption peak at high temperature is associated with the reduction of NiO species in interaction with Ru. NiO species are typically reduced at high temperatures (600 – 836 °C) [48-50]. However, the NiO reduction temperature can be reduced by Ru addition. This phenomenon, corresponding to the spillover effect, involves active H2 separating from the reduced Ru, migrating to the NiO species, and facilitating its reduction process [51].

The interaction strength between metal and hydrogen in the 5Ru/BCS and 3Ru-2Ni/BCS catalysts was assessed using temperature-programmed hydrogen desorption (H_2-TPD). The TPD profiles in Fig. 3(b) illustrate that hydrogen desorption from the 5Ru/BCS catalyst surface began at 30 °C, with the highest H_2 desorption occurring at 75 °C. Compared to the BCS supporting dual-functional hydrolysis hydrogenation (Ru/S-CCS) [31] and Ru/C [52] catalysts, the highest H_2 desorption temperature of the 5Ru/BCS catalyst was dramatically lower than that of Ru/S-CCS (165 °C) and Ru/C (419 °C). The H_2 chemisorption and spillover are associated with the H_2 desorption from the Ru catalyst surface [53]. The marginal H_2 adsorption and substantial H_2 mobility on the catalyst surface correspond to lower hydrogen desorption temperatures. Therefore, the 5Ru/BCS surface possessed greater hydrogen mobility than the Ru/S-CCS and Ru/C catalysts. On the other hand, the highest H_2 desorption temperature of the 3Ru-2Ni/BCS catalyst was observed at 115 °C, which was lower than that of the modified γ-alumina supported ruthenium-nickel catalyst [54]. These results indicate that BCS could be an outstanding metallic catalyst supporting material. Interestingly, when comparing the 5Ru/BCS and 3Ru-2Ni/BCS catalysts, it was found that the lower maximum H_2 desorption temperature and the higher maximum intensity of hydrogen desorption peaks were constituted by the 5Ru/BCS catalyst. The increase in the maximum H_2 desorption temperature and the decrease in hydrogen desorption peak intensity in the 3Ru-2Ni/BCS catalyst were primarily caused by the high H_2 desorption temperature of Ni and the low H_2 desorption quantity of the catalyst, respectively.

Surface chemical functional groups of the BCS, 5Ru/BCS, and 3Ru-2Ni/BCS samples were elucidated through FTIR spectra (Fig. S1). The BCS spectra presented similar transmission bands to those of the 5Ru/BCS and 3Ru-2Ni/BCS spectra, but some bands had different relative intensities. This indicates that the surface chemical functional groups of the BCS were only marginally changed by the metal impregnation and reduction processes. The noticeable peaks of the stretching H bonds of hydroxyl, acid, and alcohol functional groups appear at 3500 – 3400 cm^{-1} [55], and the peaks at 2925 and 2850 cm^{-1} are assigned to -CH_2 groups [56]. The bands at 1600 and 1380 cm^{-1} represent the C=C stretching vibration in aromatic rings and the C–H bending of aliphatic hydrocarbon, respectively, indicating the presence of aromatic and aliphatic compounds in the BCS, 5Ru/BCS, and 3Ru-2Ni/BCS samples [32].

The elemental compositions of BCS, 5Ru/BCS, and 3Ru-2Ni/BCS samples, along with the Ru and Ni oxidation states on 5Ru/BCS and 3Ru-2Ni/BCS surfaces, were subsequently demonstrated by XPS spectra (Fig. 4). The peaks at binding energies of 283.5 eV and 530.5 eV corresponded to C1 s and O1 s, respectively. Therefore, the wide scan in Fig. 4 revealed that the BCS, 5Ru/BCS, and 3Ru-2Ni/BCS samples primarily consisted of carbon and oxygen elements. Additionally, the 3Ru-2Ni/BCS sample showed the spectrum of Ni2p at the binding energy of 855 eV, verifying the presence of nickel. Both 5Ru/BCS and 3Ru-2Ni/BCS catalysts illustrate the band of Ru3p at the binding energy of 484.1 eV [26], indicating that the Ru element was successfully introduced to the catalysts. To explore further perception into the state of Ni and Ru on the 5Ru/BCS and 3Ru-2Ni/BCS surfaces, high-resolution XPS spectra of Ru3p and Ni2p were analyzed. The high-resolution XPS spectrum of Ru3p (Fig. 4) showed two prominent spectra at 462 and 484 eV, corresponding to $Ru3p_{3/2}$ and $Ru3p_{1/2}$, respectively, and the spectrum of Ni2p showed the outstanding peaks of both $Ni2p_{3/2}$ and $Ni2p_{1/2}$. These indicate that the 5Ru/BCS surface contained ruthenium in a zero-oxidation state, and the 3Ru-2Ni/BCS surface contained the zero-oxidation state of both ruthenium and nickel [57].

Additionally, the thermal stability analysis of BCS, 5Ru/BCS, and 3Ru-2Ni/BCS is elucidated using the curves of thermogravimetric analysis (TG) and derivative thermogravimetry (DTG) in Fig. 5(a) and (b), respectively. It can be observed that there is no substantial difference in thermal stability among BCS, 5Ru/BCS, and 3Ru-2Ni/BCS. The major mass loss at 50 – 180 °C is primarily due to moisture and volatile evaporation. A negligible mass loss at 180 – 850 °C indicates that the samples have high thermal stability. However, an in-depth comparison revealed that BCS has a marginally higher residual mass with a slightly lower mass loss rate than 5Ru/BCS and 3Ru-2Ni/BCS, implying that the presence of Ru and Ni could reduce the thermal stability of BCS.

Additionally, the structures of BCS, 5Ru/BCS, and 3Ru-2Ni/BCS were observed through XRD patterns (Fig. S2 (a)) and Raman spectra (Fig. S2 (b)). The XRD patterns of BCS, Ru/BCS, and 3Ru-2Ni/BCS show a similar broad peak at 15 – 27°, which can be attributed to the carbonaceous layer structure of graphitic materials [58]. However, the peak of Ru nanoparticles at 2θ of 43.8° disappeared in the XRD pattern of both

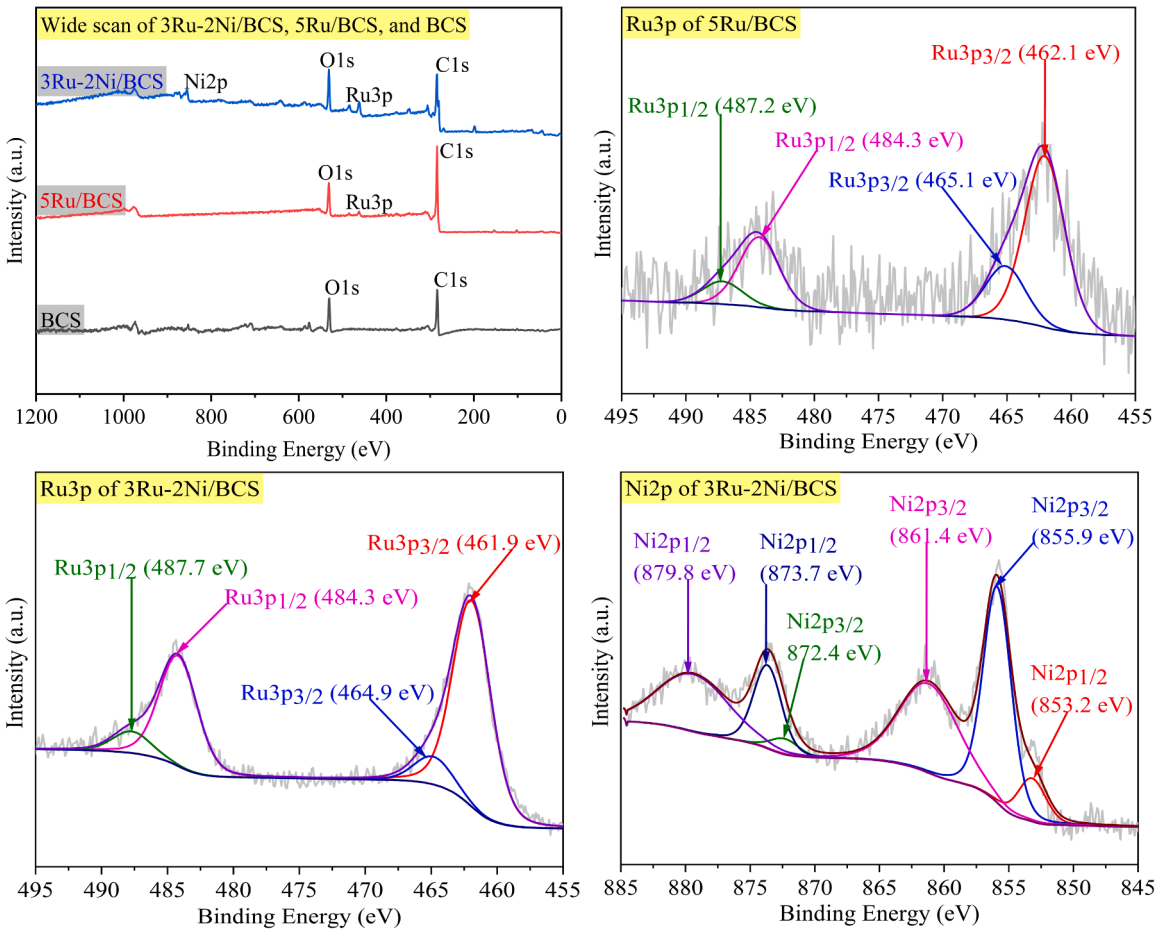

Fig. 4. XPS spectra of 3Ru-2Ni/BCS, 5Ru/BCS, and BCS.

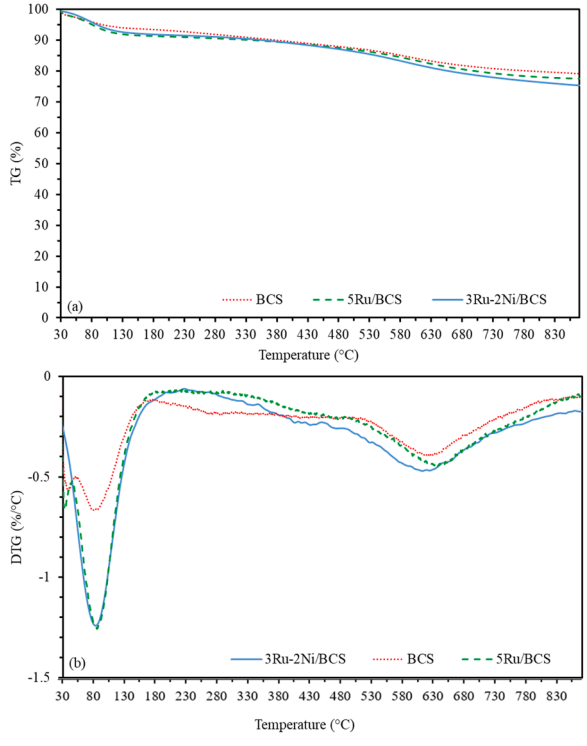

Fig. 5. (a) TG and (b) DTG curves of BCS, 5Ru/BCS, and 3Ru-2Ni/BCS.

Ru/BCS and 3Ru-2Ni/BCS catalysts, probably due to either the amorphous nature of the Ru nanoparticles or their low content and small sizes [59]. On the other hand, the peak at 2θ of 44.5°, 50.3°, and 73.8° demonstrated in the XRD patterns of 3Ru-2Ni/BCS indicates that metallic Ni (JCPDS 04–0850) was supported by the BCS [60]. Additionally, the defect sites in BCS, 5Ru/BCS, and 3Ru-2Ni/BCS were explored through Raman spectra. The D and G bands at 1357 and 1590 cm^{-1} are associated with the amount of disorder and graphitic carbon, respectively [61]. The defect sites and their concentration in the carbon matrix are typically determined by the I_D/I_G ratio [62]. In this study, the I_D/I_G ratios of BCS, 5Ru/BCS, and 3Ru-2Ni/BCS were 0.63, 0.67, 0.87, respectively. As can be seen, the I_D/I_G value of 5Ru/BCS (0.67) was higher than that of BCS (0.63), elucidating the appearance of defect sites in the carbon matrix because of the strong interaction of Ru nanoparticles with the carbon matrix [63]. Moreover, the I_D/I_G value of 3Ru-2Ni/BCS (0.87) was higher than that of both BCS and 5Ru/BCS, implying that 3Ru-2Ni/BCS contained more defect sites than 5Ru/BCS resulting from the robust synergistic interaction of Ru and Ni nanoparticles with the carbon matrix.

The surface and structure morphologies of BCS, 5Ru/BCS, and 3Ru-2Ni/BCS were explored via SEM and TEM images, respectively. The surface morphology of the pristine CS displays a smooth, plain, and flat characteristic (Fig. S3). However, after carbonization at 500 °C, the surface underwent significant changes. The BCS surface (Fig. 6(a)) displayed fractures with large holes and numerous scraps, primarily due to the devolatilization and depolymerization of the CS, consistent with the reduction in oxygen content following carbonization. Compared to the BCS, the 5Ru/BCS surface (Fig. 6(b)) was flatter and denser, possibly due to the Ru impregnation and the reduction processes altering the BCS

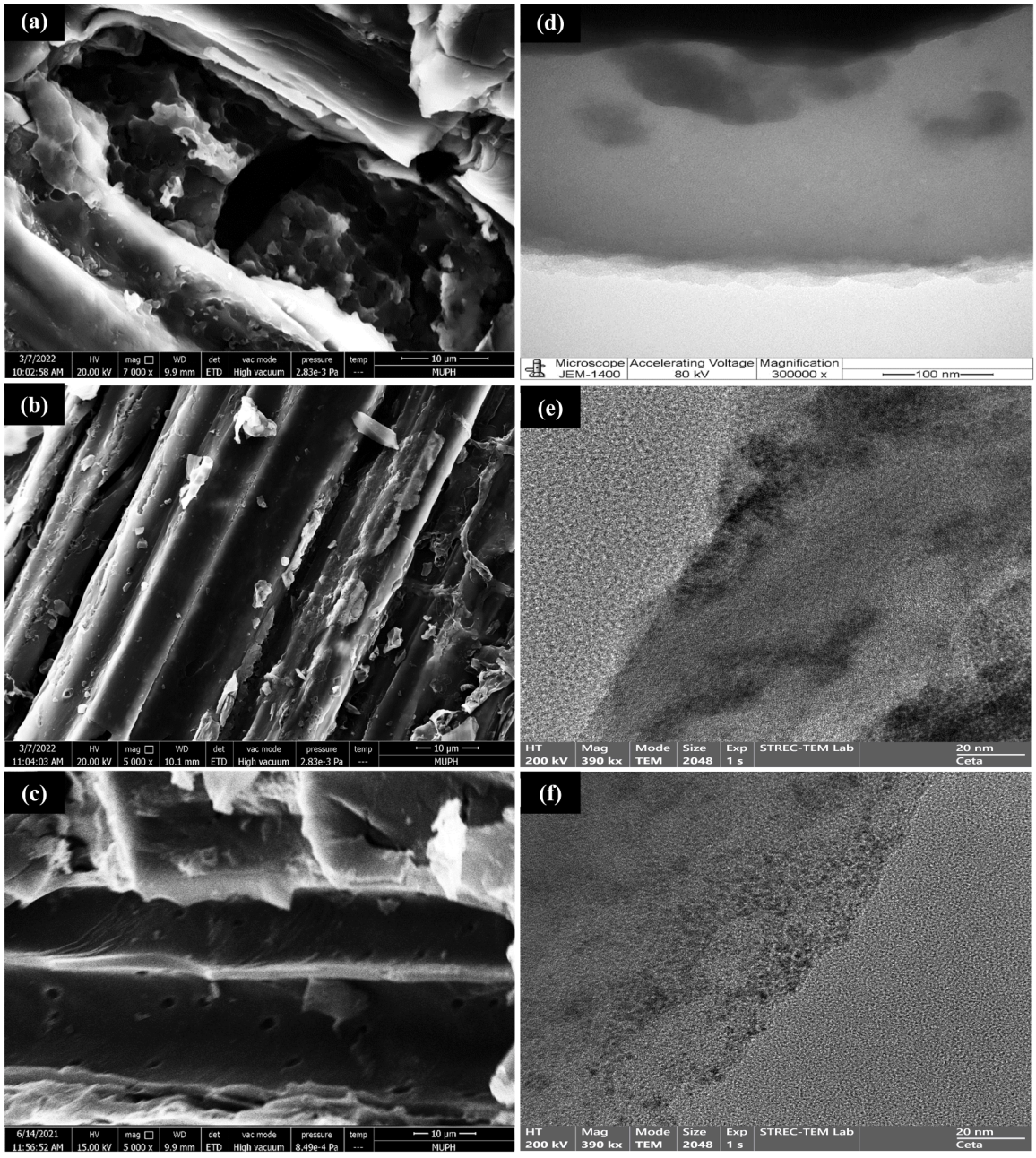

Fig. 6. SEM and TEM images of BCS, 5Ru/BCS, and 3Ru-2Ni/BCS.

surface morphology. Additionally, large grooves with pores appeared on the 3Ru-2Ni/BCS surface, mainly caused by the presence of Ni. The structure morphologies of BCS, 5Ru/BCS, and 3Ru-2Ni/BCS samples (Fig. 6(d) – (f)) illustrate that the 5Ru/BCS surface had an extensive distribution of 1.5 – 3 nm Ru nanoparticles (Fig. S4(a)), attributed to the crystalline Ru0 metallic nanoparticles [64]. When comparing, size of Ru nanoparticle on 5Ru/BCS surface was smaller than those on the cassava dregs biochar surface (4 nm) [26], indicating that BCS could be an outstanding catalyst supporting material. Interestingly, the 3Ru-2Ni/BCS surface exhibited a wide dispersion of both Ru and Ni with an average particle size of 1.5 – 3 nm (Fig. S4(b)), indicating that good dispersion of both Ru and Ni can be found on the supporting BCS material.

3.3. Catalytic activity of metal-supported biochar catalyst

To evaluate the catalytic performance of the CS-derived metal-supported biochar catalyst, the hydrogenation of xylose to xylitol was conducted under various significant parameters, including process temperature (100 – 160 °C), retention time (3 – 12 h), Ru content (1 – 5 %), and H_2 pressure (2 – 5 MPa). As shown in Fig. 7, process temperature, retention time, Ru content, and H_2 pressure constituted a noticeable impact on xylitol yield, xylitol selectivity, and xylose conversion. Fig. 7(a) illustrates that increasing the process temperature from 100 – 120 °C elevated xylitol yield, xylitol selectivity, and xylose conversion from 64.0 - 83.9 %, 91.0 - 96.4 %, and 70.4 - 87.0 %, respectively. However, further increasing the temperature to 160 °C diminished the xylitol yield and selectivity to 49.4 and 50.1 %, respectively, while raising xylose conversion to 98.7 %. The decreases in xylitol yield and selectivity were principally due to the subsequent decomposition of

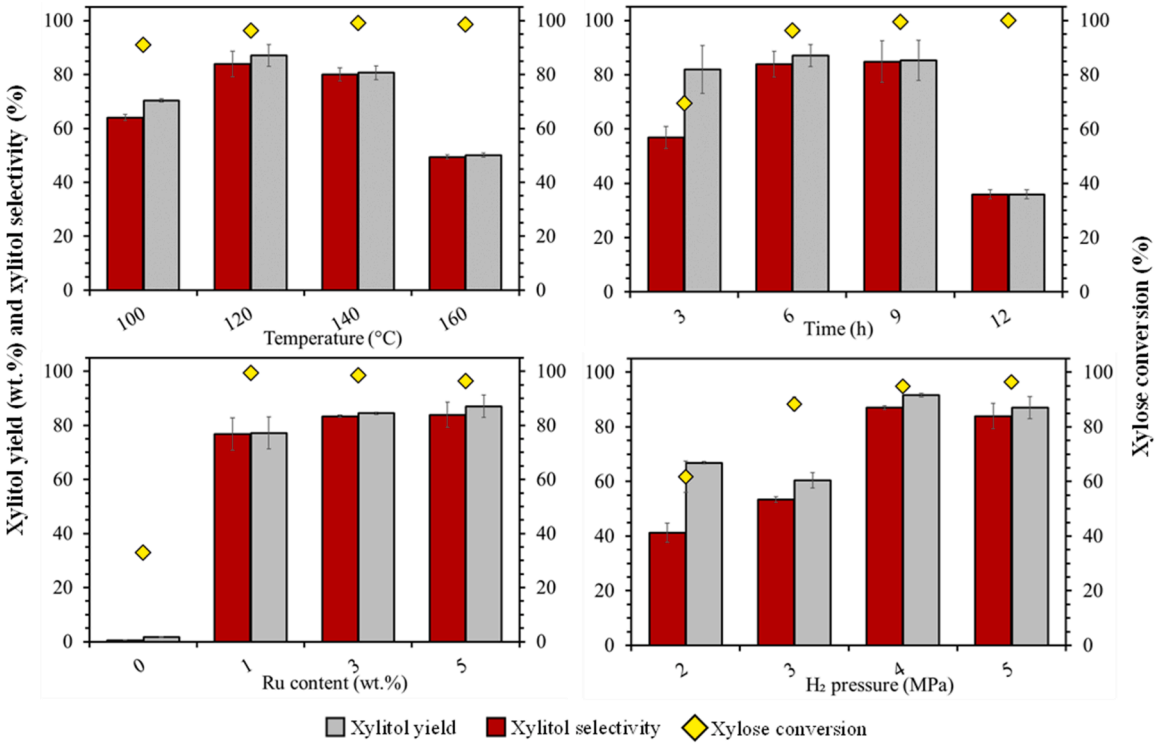

Fig. 7. Effect of reaction condition on xylitol production. (a) Effect of process temperatures (6 h retention time, 5 % Ru, 5 MPa H_2); (b) Effect of retention times (120 °C process temperature, 5 % Ru, 5 MPa H_2); (c) Effect of Ru contents (120 °C process temperature, 6 h retention time, 5 MPa H_2); (d) Effect of H_2 pressures (120 °C process temperature, 6 h retention time, 5 % Ru).

xylitol into other by-products [4,65-67]. Therefore, 120 °C was indicated as the optimal temperature for the distinguished catalytic performance of the Ru/BCS catalyst for the conversion of xylose into xylitol.

The influence of retention time on xylose hydrogenation to xylitol, shown in Fig. 7(b), indicated that increasing the retention time from 3 to 9 h enhanced xylitol yield, xylitol selectivity, and xylose conversion from 56.9 – 84.8 %, 82.0 – 85.2 %, and 69.6 – 99.5 %, respectively. When the retention time was subsequently enhanced to 12 h, xylose conversion improved to 100 %, whereas both xylitol yield and selectivity declined to 35.9 %. Interestingly, a retention time of 6 h for xylose hydrogenation resulted in a xylose conversion of 96.4 % and a xylitol yield of 83.9 %, which were only slightly lower than those obtained with a retention time of 9 h Therefore, to reduce resource expenditures, 6 h was identified as the optimal retention time for xylose hydrogenation using the Ru/BCS catalyst.

Subsequently, the influences of Ru content on xylitol yield, xylitol selectivity, and xylose conversion are elucidated in Fig. 8(c). It can be noted that increasing Ru content from 1 to 5 % enhanced xylitol yield and selectivity from 76.8 to 83.9 % and from 77.2 to 87.0 %, respectively, while xylose conversion remained unchanged.

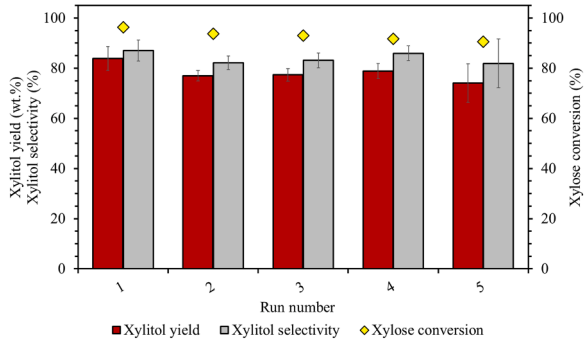

Fig. 8. Recycling performance of Ru/BCS catalyst.

Similarly, Fig. 7(d) shows the effect of H_2 pressure on xylose hydrogenation to xylitol. It can be observed that raising the H_2 pressure from 2 to 4 MPa increased xylitol yield, xylitol selectivity, and xylose conversion from 41.3 – 87.0 %, 66.8 – 91.6, and 61.8 – 94.9 %, respectively. When the H_2 pressure was further increased to 5 MPa, xylose conversion slightly enhanced to 96.4 %, but the xylitol yield and selectivity marginally reduced to 83.9 and 87.0 %, respectively. Hence, the above results identified that the notable catalytic performance of the Ru/BCS for the conversion of xylose into xylitol was determined at 120 °C for 6 h with 5 % Ru content under 4 MPa H_2.

The durability and reusability of the Ru/BCS catalyst are crucial factors for efficient xylitol production. In this study, these properties of the Ru/BCS catalyst were assessed under the optimal reaction conditions. Following the reaction, the spent catalyst was segregated from the liquid product, washed, and dried. This spent catalyst was mixed with 0.05 g of fresh Ru/BCS and subsequently used for the subsequent reaction of 1 g xylose hydrogenation. The recycling experiment results are shown in Fig. 8. It was noted that the xylitol yield, selectivity, and xylose conversion slightly reduced with each consecutive experiment. An initial xylitol yield of 83.5 % and selectivity of 86.8 % were deemed acceptable, with a reduction within approximately 5 %. However, xylitol yield, xylitol selectivity, and xylose conversion were reduced in the second recycling run and remained nearly stable between the second and fifth recycling runs. The decrease in xylitol yield, xylitol selectivity, and xylose conversion in the first recycling experiments could be caused by the adsorption and accumulation of humins or by-products on the catalyst's metal sites [26,31], as indicated by the decrease of SSA, pore size, and pore volume (Table 2 and Fig. S5) with increasing carbon content. Moreover, the rapid decrease of Ru content in the spent Ru/BCS catalyst to 0.03 wt.% and the appearance of Ru in the liquid product (0.052 mg/L) could significantly contribute to the decline in catalytic performance. Additionally, the TEM image of the spent Ru/BCS in Fig. S6 confirms the catalyst agglomeration, further contributing to

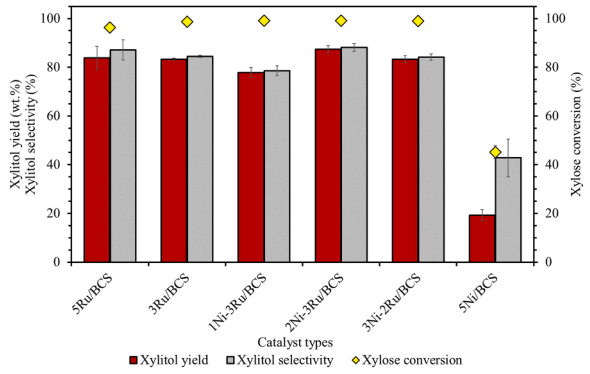

Fig. 9. Effect of Ni element on xylitol production (120 °C process temperature, 6 h retention time, 5 MPa H_2).

deactivation. Nevertheless, char surface modification and catalyst regeneration strategies could improve the longevity of the Ru/BCS catalyst. Modifying the char surface with functional groups (e.g., carboxyl, hydroxyl, and phosphorous) can improve the anchoring of Ru particles, enhancing adhesion and preventing leaching [31,68]. Furthermore, thermal and chemical regeneration techniques (e.g., acid, base, or ethanol treatment) can effectively eliminate the adsorbed species and regenerate the catalyst's active sites without causing sintering or Ru loss [31,68].

3.4. Effect of ni element on xylitol production

To elevate the efficacy of the single metallic Ru-supported biochar catalyst in the xylose hydrogenation reaction, the efficacy of a bimetallic Ru-Ni-supported biochar catalyst in xylitol production was explored. As shown in Fig. 9, the use of the 3Ru/BCS catalyst achieved 83.3 % xylitol yield and 98.6 % xylose conversion, which were noticeably higher than those of the 5Ni/BCS catalyst. On the other hand, 87.4 % xylitol yield and 99.1 % xylose conversion were derived using the bimetallic catalyst of 2Ni-3Ru/CCS, which were higher than those of the monometallic catalysts of 5Ru/BCS and 3Ru/BCS. These results indicate that the synergistic effect between Ru and Ni nanoparticles in the 2Ni-3Ru/CCS catalyst had a significant impact on elevating xylitol yield in the xylose hydrogenation reaction. The synergistic effect between Ru and Ni nanoparticles was also reported in direct sorbitol production from cellulose [43]. However, the amount of Ni should be optimized. The interaction between Ru, Ni, and biochar enhances the overall hydrogenation process by improving hydrogen activation, providing better metal stability, and tuning reaction selectivity. Ru has excellent hydrogen dissociation abilities [69], and Ni can enhance hydrogen transfer to the substrate [70]. The strong interaction of Ru and Ni can improve catalytic activity by increasing hydrogen availability at the active sites. On the other hand, biochar surfaces often contain oxygen-containing functional groups that can influence metal-support interactions. These groups can enhance the anchoring of Ru and Ni particles, improving their dispersion and possibly enhancing catalytic activity by modifying the electronic properties of the metals [20]. Additionally, the combination of Ru and Ni on biochar can promote hydrogen spillover, where hydrogen atoms dissociated on Ru migrate to Ni and the biochar support. This process increases the effective surface area for hydrogenation, allowing more substrate molecules to be hydrogenated simultaneously.

The efficacy of hydrogenation catalysis of the metallic catalysts is presented in Table 3. In comparison, the 5 % Ru/BCS catalyst had similar catalytic activity to the commercial 5 % Ru/C catalyst. Surprisingly, the 3 % Ru-2 % Ni/BCS catalyst demonstrated higher catalytic performance than both the 5 % Ru/BCS and 5 % Ru/C catalysts. Therefore, the results of this study indicate that BCS can be a competitive metallic catalyst supporting material for xylose hydrogenation into xylitol. In addition, the 5 % Ru/BCS was employed for xylitol production from hydrolysates enriched with CS xylose, which were prepared via the 0.5 % HNO_3 hydrolysis pretreatment of CS at 140 °C for 1 h and detoxification using the method reported in a relevant study [72]. The obtained detoxified hydrolysates contained xylose reaching 17.2 g/L, and the hydrogenation of the hydrolysates at 120 °C for 6 h under 5 MPa H_2 using 5 % Ru/BCS and 5 % Ru/C catalysts derived 3.2 % and 24.9 % xylitol yield, respectively. The low xylitol yield of both the 5 % Ru/BCS and 5 % Ru/C catalysts could be due to hydrolysate contaminants.

4. Conclusion

A novel utilization strategy for the plentiful corn stover (CS) waste was proposed, using it as a valuable biomass-based biochar support for a metallic catalyst in the hydrogenation of xylose into xylitol. The synthesized single- and bi-metallic catalysts, including 5Ru/BCS and 3Ru-2Ni/BCS, demonstrated dominant efficacy for the hydrogenation of xylose into xylitol. The 5Ru/BCS catalyst achieved the highest xylitol

Table 3
Comparison of various metal-based catalysts for xylitol production from xylose and hydrolysates enriched xylose.

Catalysts	Feedstock	Xylitol production			Xylitol yield (%)	Xylitol selectivity (%)	Reference
		Reaction temperature (°C)	Reaction time (h)	H_2 pressure (MPa)			
5 %Ru/BCS	Xylose	120	6	5	83.9	87.0	This study
3 %Ru-2 %Ni/BCS	Xylose	120	6	5	87.4	88.2	This study
3 %Ru/BCS	Xylose	120	6	5	83.3	84.5	This study
5 %Ru/C	Xylose	120	6	5	48.2	48.2	This study
5 %Ru/C	Xylose	80	3	5	84.2	87.2	This study
5 %Ru/BCS	Hydrolysates enriched CS xylose	120	6	5	3.2	3.4	This study
5 %Ru/C	Hydrolysates enriched CS xylose	120	6	5	24.9	37.5	This study
1 %Ru/C	Xylose	120	2	5.5	97.5	94.0	[16]
1 %Ru/MWCNT[a]	Xylose	130	6	3[c]	84.0	71.0	[71]
3 %Ru/CF[b]	Xylose	110	1.5	5	98.1	98.2	[66]
1 %Ru-5 %Ni/C	Hydrolysates enrich bagasse xylose	100	1	3.45	NA[d]	90.0	[72]

[a] MWCNT: multiwall carbon nanotubes.
[b] CF: carbon foam.
[c] Using H_2O:2-propanol (1:1) as solvent mixture.
[d] NA: not available.

yield and selectivity of 87.0 % and 91.6 %, respectively, at 120 °C for 6 h under 4 MPa H_2. Several characterization techniques demonstrated that the catalyst possessed metal active sites for hydrogenation reaction. A synergistic effect between Ru and Ni nanoparticles in the 3Ru-2Ni/BCS catalyst resulted in a xylitol yield of 87.4 wt.%, with xylitol selectivity and xylose conversion of 88.2 % and 99.1 %, respectively. These results indicate that biochar CS is efficient for use as a metallic catalyst supporting material for xylose hydrogenation into xylitol.

Data availability

Data will be made available on request.

CRediT authorship contribution statement

Kridsada Karin: Writing – original draft, Visualization, Methodology, Investigation, Formal analysis, Data curation. **Sanchai Kuboon:** Resources, Methodology. **Bunyarit Panyapinyopol:** Supervision, Resources, Methodology. **Saran Youngjan:** Formal analysis. **Wanwitoo Wanmolee:** Resources, Methodology. **Nawin Viriya-empikul:** Writing – review & editing, Supervision, Methodology, Conceptualization. **Navadol Laosiripojana:** Writing – review & editing, Supervision, Methodology, Funding acquisition, Formal analysis, Conceptualization. **Kamonwat Nakason:** Writing – review & editing, Writing – original draft, Visualization, Supervision, Resources, Project administration, Methodology, Funding acquisition, Data curation, Conceptualization, Validation.

Declaration of competing interest

The authors declare that they have no known competing financial interests or personal relationships that could have appeared to influence the work reported in this paper.

Acknowledgement

This research project is supported by Specific League Funds from Mahidol University, and partially supported by Office of the Permanent Secretary, Ministry of Higher Education, Science, Research and Innovation (OPS MHESI), Thailand Science Research and Innovation (TSRI) (Grant No. RGNS 63 – 167). We thank Mahidol University Frontier Research Facility (MU-FRF) for instrument support and the MU-FRF scientists, Nawapol Udpuay, Dr. Suwilai Chaveanghong and Bancha Panyacharoen, for their kind assistance in operation of the simultaneous thermogravimetric analyzer and the X-ray diffractometer (XRD).

Supplementary materials

Supplementary material associated with this article can be found, in the online version, at doi:10.1016/j.recm.2024.10.002.

References

[1] Y. Jin, S. Hu, Z. Zhang, B. Zhu, D. Bai, The path to carbon neutrality in China: a paradigm shift in fossil resource utilization, Resour. Chem. Mater. 1 (2022) 129–135, https://doi.org/10.1016/j.recm.2022.01.003.

[2] D. Zhao, R. Li, L. Shi, X. Zeng, W. Zhang, R. Wu, Z. Han, Y. Sun, G. Xu, Tendencies of research and development in resources chemicals and materials — Summarization of a Youth's topic forum, Resour. Chem. Mater. 2 (2023) 215–222, https://doi.org/10.1016/j.recm.2023.04.002.

[3] H. Xiang, R. Xin, N. Prasongthum, P. Natewong, T. Sooknoi, J. Wang, P. Reubroycharoen, X. Fan, Catalytic conversion of bioethanol to value-added chemicals and fuels: a review, Resour. Chem. Mater. 1 (2022) 47–68, https://doi.org/10.1016/j.recm.2021.12.002.

[4] Y. Delgado Arcaño, O.D. Valmaña García, D. Mandelli, W.A. Carvalho, L. A. Magalhães Pontes, Xylitol: a review on the progress and challenges of its production by chemical route, Catal. Today. (2018), https://doi.org/10.1016/j.cattod.2018.07.060.

[5] A. Bayu, M.F. Warsito, M.Y. Putra, S. Karnjanakom, G. Guan, Macroalgae-derived rare sugars: applications and catalytic synthesis, Carbon Resour. Convers. 4 (2021) 150–163, https://doi.org/10.1016/j.crcon.2021.04.002.

[6] D. Dasgupta, S. Bandhu, D.K. Adhikari, D. Ghosh, Challenges and prospects of xylitol production with whole cell bio-catalysis: a review, Microbiol. Res. 197 (2017) 9–21, https://doi.org/10.1016/j.micres.2016.12.012.

[7] T.L.d. Albuquerque, I.J.D. Silva, G.R. de Macedo, M.V.P. Rocha, Biotechnological production of xylitol from lignocellulosic wastes: a review, Process Biochem. 49 (2014) 1779–1789, https://doi.org/10.1016/j.procbio.2014.07.010.

[8] L. Venkateswar Rao, J.K. Goli, J. Gentela, S. Koti, Bioconversion of lignocellulosic biomass to xylitol: an overview, Bioresour. Technol. 213 (2016) 299–310, https://doi.org/10.1016/j.biortech.2016.04.092.

[9] M. Herskowitz, Modelling of a trickle-bed reactor—the hydrogenation of xylose to xylitol, Chem. Eng. Sci. 40 (1985) 1309–1311, https://doi.org/10.1016/0009-2509(85)85091-0.

[10] K. van Gorp, E. Boerman, C.V. Cavenaghi, P.H. Berben, Catalytic hydrogenation of fine chemicals: sorbitol production, Catal. Today. 52 (1999) 349–361, https://doi.org/10.1016/S0920-5861(99)00087-5.

[11] J.P. Mikkola, T. Salmi, Three-phase catalytic hydrogenation of xylose to xylitol — Prolonging the catalyst activity by means of on-line ultrasonic treatment, Catal. Today. 64 (2001) 271–277, https://doi.org/10.1016/S0920-5861(00)00530-7.

[12] J.-P. Mikkola, H. Vainio, T. Salmi, R. Sjöholm, T. Ollonqvist, J. Väyrynen, Deactivation kinetics of Mo-supported Raney Ni catalyst in the hydrogenation of xylose to xylitol, Appl. Catal. 196 (2000) 143–155, https://doi.org/10.1016/S0926-860X(99)00453-6.

[13] J.-P. Mikkola, R. Sjöholm, T. Salmi, P. Mäki-Arvela, Xylose hydrogenation: kinetic and NMR studies of the reaction mechanisms, Catal. Today. 48 (1999) 73–81, https://doi.org/10.1016/S0920-5861(98)00360-5.

[14] P. Gallezot, N. Nicolaus, G. Flèche, P. Fuertes, A. Perrard, Glucose hydrogenation on ruthenium catalysts in a trickle-bed reactor, J. Catal. 180 (1998) 51–55, https://doi.org/10.1006/jcat.1998.2261.

[15] C. Hernandez-Mejia, E.S. Gnanakumar, A. Olivos-Suarez, J. Gascon, H.F. Greer, W. Zhou, G. Rothenberg, N.R. Shiju, Ru/TiO2-catalysed hydrogenation of xylose: the role of the crystal structure of the support, Catal. Sci. Technol. 6 (2016) 577–582, https://doi.org/10.1039/C5CY01005E.

[16] M. Yadav, D.K. Mishra, J.-S. Hwang, Catalytic hydrogenation of xylose to xylitol using ruthenium catalyst on NiO modified TiO2 support, Appl. Catal. 425-426 (2012) 110–116, https://doi.org/10.1016/j.apcata.2012.03.007.

[17] D.K. Mishra, A.A. Dabbawala, J.J. Park, S.H. Jhung, J.-S. Hwang, Selective hydrogenation of d-glucose to d-sorbitol over HY zeolite supported ruthenium nanoparticles catalysts, Catal. Today. 232 (2014) 99–107, https://doi.org/10.1016/j.cattod.2013.10.018.

[18] K. Nakason, P. Sumrannit, S. Youngjan, W. Wanmolee, W. Kraithong, P. Khemthong, V. Kanokkantapong, B. Panyapinyopol, Environmental impact of 5-hydroxymethylfurfural production from cellulosic sugars using biochar-based acid catalyst, Chem. Eng. Sci. 287 (2024) 119729, https://doi.org/10.1016/j.ces.2024.119729.

[19] C. Lokmit, K. Nakason, S. Kuboon, A. Jiratanachotikul, B. Panyapinyopol, A comparison of char fuel properties derived from dry and wet torrefaction of oil palm leaf and its techno-economic feasibility, Mater. Sci. Energy Technol. 6 (2023) 192–204, https://doi.org/10.1016/j.mset.2022.12.010.

[20] S. Wang, H. Li, M. Wu, Advances in metal/biochar catalysts for biomass hydro-upgrading: a review, J. Clean. Prod. 303 (2021) 126825, https://doi.org/10.1016/j.jclepro.2021.126825.

[21] S.-F. Jiang, L.-L. Ling, Z. Xu, W.-J. Liu, H. Jiang, Enhancing the Catalytic Activity and Stability of Noble Metal Nanoparticles by the Strong Interaction of Magnetic Biochar Support, Ind. Eng. Chem. Res. 57 (2018) 13055–13064, https://doi.org/10.1021/acs.iecr.8b02777.

[22] P. Veerakumar, I. Panneer Muthuselvam, C.-T. Hung, K.-C. Lin, F.-C. Chou, S.-B. Liu, Biomass-Derived Activated Carbon Supported Fe3O4 Nanoparticles as Recyclable Catalysts for Reduction of Nitroarenes, ACS Sustain. Chem. Eng. 4 (2016) 6772–6782, https://doi.org/10.1021/acssuschemeng.6b01727.

[23] A.L. Jongerius, R.W. Gosselink, J. Dijkstra, J.H. Bitter, P.C.A. Bruijnincx, B. M. Weckhuysen, Carbon Nanofiber Supported Transition-Metal Carbide Catalysts for the Hydrodeoxygenation of Guaiacol, ChemCatChem 5 (2013) 2964–2972, https://doi.org/10.1002/cctc.201300280.

[24] J. Sun, A.M. Karim, H. Zhang, L. Kovarik, X.S. Li, A.J. Hensley, J.-S. McEwen, Y. Wang, Carbon-supported bimetallic Pd–Fe catalysts for vapor-phase hydrodeoxygenation of guaiacol, J. Catal. 306 (2013) 47–57, https://doi.org/10.1016/j.jcat.2013.05.020.

[25] C. Zhu, H. Wang, H. Li, B. Cai, W. Lv, C. Cai, C. Wang, L. Yan, Q. Liu, L. Ma, Selective Hydrodeoxygenation of 5-Hydroxymethylfurfural to 2,5-Dimethylfuran over Alloyed Cu−Ni Encapsulated in Biochar Catalysts, ACS Sustain. Chem. Eng. 7 (2019) 19556–19569, https://doi.org/10.1021/acssuschemeng.9b04645.

[26] Z. Li, Y. Liu, C. Liu, S. Wu, W. Wei, Direct conversion of cellulose into sorbitol catalyzed by a bifunctional catalyst, Bioresour. Technol. 274 (2019) 190–197, https://doi.org/10.1016/j.biortech.2018.11.089.

[27] L.O. Pordesimo, B.R. Hames, S. Sokhansanj, W.C. Edens, Variation in corn stover composition and energy content with crop maturity, Biomass Bioenergy 28 (2005) 366–374, https://doi.org/10.1016/j.biombioe.2004.09.003.

[28] Department of Alternative Energy Development and Efficiency, Ministry of Energy, Thailand, Biomass potential in 2013. http://biomass.dede.go.th/biomass_web/index.html. (accessed 25 June 2024).

[29] O. Erenstein, M. Jaleta, K. Sonder, K. Mottaleb, B.M. Prasanna, Global maize production, consumption and trade: trends and R&D implications, Food Secur. 14 (2022) 1295–1319, https://doi.org/10.1007/s12571-022-01288-7.

[30] S. Yang, Y. Zhang, W. Yue, W. Wang, Y.-Y. Wang, T.-Q. Yuan, R.-C. Sun, Valorization of lignin and cellulose in acid-steam-exploded corn stover by a moderate alkaline ethanol post-treatment based on an integrated biorefinery concept, Biotechnol. Biofuels. 9 (2016) 238, https://doi.org/10.1186/s13068-016-0656-1.

[31] R. Soda, W. Wanmolee, B. Panyapinyopol, P. Boonyoung, W. Kraithong, N. Viriya-empikul, N. Laosiripojana, K. Nakason, Corn stover-derived biochar supporting dual functional catalyst for direct sorbitol production from cellulosic materials, Clean. Mater. 13 (2024) 100254, https://doi.org/10.1016/j.clema.2024.100254.

[32] K. Nakason, P. Chukaew, F. Utrarachkij, S. Kuboon, W. Kraithong, S. Pichaiyut, W. Wanmolee, B. Panyapinyopol, Antimicrobial and antioxidant activities of lignin by-product from sugarcane leaf conversion to levulinic acid and hydrochar, Sustain. Mater. Technol. 40 (2024) e00973, https://doi.org/10.1016/j.susmat.2024.e00973.

[33] Sluiter, A., Hames, B., Ruiz, R., Scarlata, C., Sluiter, J., Templeton, D., Crocker, D. Determination of structural carbohydrates and lignin in biomass (NREL/TP-510-42618). The US National Renewable Energy Laboratory technical report.

[34] Sluiter, A., Hames, B., Ruiz, R., Scarlata, C., Sluiter, J., Templeton, D. (2008) Determination of ash in biomass (NREL/TP-510-42622). The US national renewable energy laboratory technical report.

[35] ASTM, Standard Test Method For Determination of Total Solids in Biomass. Method E1756-08, ASTM International, Pennsylvania, 2010.

[36] ASTM, Standard Test Methods For Proximate Analysis of Coal and Coke by Macro Thermogravimetric Analysis. Method D7582-10, ASTM International, Pennsylvania, 2010.

[37] K. Nakason, B. Panyapinyopol, V. Kanokkantapong, N. Viriya-empikul, W. Kraithong, P. Pavasant, Characteristics of hydrochar and hydrothermal liquid products from hydrothermal carbonization of corncob, Biomass Convers. Biorefin. 8 (2018) 199–210, https://doi.org/10.1007/s13399-017-0279-1.

[38] K. Nakason, B. Panyapinyopol, V. Kanokkantapong, N. Viriya-empikul, W. Kraithong, P. Pavasant, Characteristics of hydrochar and liquid fraction from hydrothermal carbonization of cassava rhizome, J. Energy Inst. 91 (2018) 184–193, https://doi.org/10.1016/j.joei.2017.01.002.

[39] R. Xi, Y. Tang, R.L. Smith, X. Liu, L. Liu, X. Qi, Selective hydrogenation of glucose to sorbitol with tannic acid-based porous carbon sphere supported Ni–Ru bimetallic catalysts, Green Energy Environ (2022), https://doi.org/10.1016/j.gee.2022.04.003.

[40] R. Shu, H. Jiang, L. Xie, X. Liu, T. Yin, Z. Tian, C. Wang, Y. Chen, Efficient hydrodeoxygenation of lignin-derived phenolic compounds by using Ru-based biochar catalyst coupled with silicotungstic acid, Renew. Energy. 202 (2023) 1160–1168, https://doi.org/10.1016/j.renene.2022.11.092.

[41] X. Yuan, Y. Cao, J. Li, A.K. Patel, C.-D. Dong, X. Jin, C. Gu, A.C.K. Yip, D.C. W. Tsang, Y.S. Ok, Recent advancements and challenges in emerging applications of biochar-based catalysts, Biotechnol. Adv. 67 (2023) 108181, https://doi.org/10.1016/j.biotechadv.2023.108181.

[42] L. Cao, Q. Luo, J. Chen, L. Wang, Y. Lin, H. Wang, X. Liu, X. Shen, W. Zhang, W. Liu, Z. Qi, Z. Jiang, J. Yang, T. Yao, Dynamic oxygen adsorption on single-atomic Ruthenium catalyst with high performance for acidic oxygen evolution reaction, Nat. Commun. 10 (2019) 4849, https://doi.org/10.1038/s41467-019-12886-z.

[43] L.S. Ribeiro, J.J. Delgado, J.J.M. Órfão, M.F.R. Pereira, Carbon supported Ru-Ni bimetallic catalysts for the enhanced one-pot conversion of cellulose to sorbitol, Appl. Catal. B: Environ. 217 (2017) 265–274, https://doi.org/10.1016/j.apcatb.2017.04.078.

[44] C. Newman, X. Zhou, B. Goundie, I.T. Ghampson, R.A. Pollock, Z. Ross, M. C. Wheeler, R.W. Meulenberg, R.N. Austin, B.G. Frederick, Effects of support identity and metal dispersion in supported ruthenium hydrodeoxygenation catalysts, Appl. Catal. 477 (2014) 64–74, https://doi.org/10.1016/j.apcata.2014.02.030.

[45] V.A. Mazzieri, P.C. L'Argentière, F. Coloma-Pascual, N.S. Fígoli, Effect of Chlorine on the Properties of Ru/Al2O3, Ind. Eng. Chem. Res. 42 (2003) 2269–2272, https://doi.org/10.1021/ie0209428.

[46] V. Mazzieri, F. Coloma-Pascual, A. Arcoya, P.C. L'Argentière, x Fı, N.S. goli, XPS, FTIR and TPR characterization of Ru/Al2O3 catalysts, Appl. Surf. Sci. 210 (2003) 222–230, https://doi.org/10.1016/S0169-4332(03)00146-6.

[47] X. Wang, G. Lan, H. Liu, Y. Zhu, Y. Li, Effect of acidity and ruthenium species on catalytic performance of ruthenium catalysts for acetylene hydrochlorination, Catal. Sci. Technol. 8 (2018) 6143–6149, https://doi.org/10.1039/C8CY01677A.

[48] S. Andraos, R. Abbas-Ghaleb, D. Chlala, A. Vita, C. Italiano, M. Laganà, L. Pino, M. Nakhl, S. Specchia, Production of hydrogen by methane dry reforming over ruthenium-nickel based catalysts deposited on Al2O3, MgAl2O4, and YSZ, Int. J. Hydrogen Energy. 44 (2019) 25706–25716, https://doi.org/10.1016/j.ijhydene.2019.08.081.

[49] L.P.R. Profeti, J.A.C. Dias, J.M. Assaf, E.M. Assaf, Hydrogen production by steam reforming of ethanol over Ni-based catalysts promoted with noble metals, J. Power Sources. 190 (2009) 525–533, https://doi.org/10.1016/j.jpowsour.2008.12.104.

[50] Z. Yaakob, A. Bshish, A. Ebshish, S.M. Tasirin, F.H. Alhasan, Hydrogen Production by Steam Reforming of Ethanol over Nickel Catalysts Supported on Sol Gel Made Alumina: influence of Calcination Temperature on Supports, Materials (Basel) 6 (6) (2013) 2229–2239, https://doi.org/10.3390/ma6062229.

[51] N.N. Mohd Arif, S.Z. Abidin, O.U. Osazuwa, D.-V.N. Vo, M.T. Azizan, Y.H. Taufiq-Yap, Hydrogen production via CO2 dry reforming of glycerol over ReNi/CaO catalysts, Int. J. Hydrogen Energy. 44 (2019) 20857–20871, https://doi.org/10.1016/j.ijhydene.2018.06.084.

[52] M. Jędrzejczyk, E. Soszka, J. Goscianska, M. Kozanecki, J. Grams, A.M. Ruppert, The Influence of Carbon Nature on the Catalytic Performance of Ru/C in Levulinic Acid Hydrogenation with Internal Hydrogen Source, Molecules 25 (22) (2020) 5362, https://doi.org/10.3390/molecules25225362.

[53] B. Lin, R. Wang, X. Yu, J. Lin, F. Xie, K. Wei, Physicochemical Characterization and H2-TPD Study of Alumina Supported Ruthenium Catalysts, Catal. Letters. 124 (2008) 178–184, https://doi.org/10.1007/s10562-008-9483-8.

[54] A. Álvarez Moreno, T. Ramirez-Reina, S. Ivanova, A.-C. Roger, M.Á. Centeno, J. A. Odriozola, Bimetallic Ni–Ru and Ni–*Re* Catalysts for Dry Reforming of Methane: understanding the Synergies of the Selected Promoters, Front. chem. 9 (2021), https://doi.org/10.3389/fchem.2021.694976.

[55] K.-L. Chang, S.C. Muega, B.I.G. Ofrasio, W.-H. Chen, E.G. Barte, R.R.M. Abarca, M. D.G. de Luna, Synthesis of 5-hydroxymethylfurfural from glucose, fructose, cellulose and agricultural wastes over sulfur-doped peanut shell catalysts in ionic liquid, Chemosphere 291 (2022) 132829, https://doi.org/10.1016/j.chemosphere.2021.132829.

[56] L. Liu, X. Yang, Q. Hou, S. Zhang, M. Ju, Corn stalk conversion into 5-hydroxymethylfurfural by modified biochar catalysis in a multi-functional solvent, J. Clean. Prod. 187 (2018) 380–389, https://doi.org/10.1016/j.jclepro.2018.03.234.

[57] Y. Zhang, G. Zhang, T. Chen, Efficient one-pot conversion of cellulose to sorbitol over Ni-based carbon catalysts with embedment structure, Fuel 339 (2023) 127447, https://doi.org/10.1016/j.fuel.2023.127447.

[58] T.S. Pessôa, L.E.d.Lima Ferreira, M.P. da Silva, L.M. Pereira Neto, B.F. d. Nascimento, T.J.M. Fraga, E.F. Jaguaribe, J.V. Cavalcanti, M.A. da Motta Sobrinho, Açaí waste beneficing by gasification process and its employment in the treatment of synthetic and raw textile wastewater, J. Clean. Prod. 240 (2019) 118047, https://doi.org/10.1016/j.jclepro.2019.118047.

[59] N. Kryvutsa, P. Eloy, B. Hackens, S. Hermans, Synthesis of Ru, Ni and Fe supported graphene nanoplatelets catalysts for hydrogenation of glucose into sorbitol, Mol. Catal. 545 (2023) 113222, https://doi.org/10.1016/j.mcat.2023.113222.

[60] X. Ding, X. Liu, J. Cheng, D. Li, T. Li, Z. Jiang, Y. Guo, Boosted photothermal synergistic CO2 methanation over Ru doped Ni/ZrO2 catalyst: from experimental to DFT studies, Fuel 357 (2024) 129779, https://doi.org/10.1016/j.fuel.2023.129779.

[61] J.-B. Wu, M.-L. Lin, X. Cong, H.-N. Liu, P.-H. Tan, Raman spectroscopy of graphene-based materials and its applications in related devices, Chem. Soc. Rev. 47 (2018) 1822–1873, https://doi.org/10.1039/C6CS00915H.

[62] N. Shimodaira, A. Masui, Raman spectroscopic investigations of activated carbon materials, J. Appl. Phys. 92 (2002) 902–909, https://doi.org/10.1063/1.1487434.

[63] M. Gopiraman, S.G. Babu, Z. Khatri, K. Wei, M. Endo, R. Karvembu, I.S. Kim, Facile and homogeneous decoration of RuO2 nanorods on graphene nanoplatelets for transfer hydrogenation of carbonyl compounds, Catal. Sci. Technol. 3 (2013) 1485–1489, https://doi.org/10.1039/C3CY20735H.

[64] P.A. Lazaridis, S. Karakoulia, A. Delimitis, S.M. Coman, V.I. Parvulescu, K. S. Triantafyllidis, D-Glucose hydrogenation/hydrogenolysis reactions on noble metal (Ru, Pt)/activated carbon supported catalysts, Catal. Today. 257 (2015) 281–290, https://doi.org/10.1016/j.cattod.2014.12.006.

[65] K. Dietrich, C. Hernandez-Mejia, P. Verschuren, G. Rothenberg, N.R. Shiju, One-Pot Selective Conversion of Hemicellulose to Xylitol, Org. Process Res. Dev. 21 (2017) 165–170, https://doi.org/10.1021/acs.oprd.6b00169.

[66] T.N. Pham, A. Samikannu, A.-R. Rautio, K.L. Juhasz, Z. Konya, J. Wärnå, K. Kordas, J.-P. Mikkola, Catalytic Hydrogenation of D-Xylose Over Ru Decorated Carbon Foam Catalyst in a SpinChem® Rotating Bed Reactor, Top. Catal. 59 (2016) 1165–1177, https://doi.org/10.1007/s11244-016-0637-4.

[67] G. Yi, Y. Zhang, One-Pot Selective Conversion of Hemicellulose (Xylan) to Xylitol under Mild Conditions, ChemSusChem 5 (2012) 1383–1387, https://doi.org/10.1002/cssc.201200290.

[68] M. Qiu, J. Zheng, Y. Yao, L. Liu, X. Zhou, H. Jiao, J. Aarons, K. Zhang, Q. Guan, W. Li, Directly converting cellulose into high yield sorbitol by tuning the electron structure of Ru2P anchored in agricultural straw biochar, J. Clean. Prod. 362 (2022) 132364, https://doi.org/10.1016/j.jclepro.2022.132364.

[69] F. Rose, M. Tatarkhanov, E. Fomin, M. Salmeron, Nature of the Dissociation Sites of Hydrogen Molecules on Ru(001), J. Phys. Chem. C. 111 (2007) 19052–19057, https://doi.org/10.1021/jp075787v.

[70] F. Alonso, P. Riente, M. Yus, Nickel Nanoparticles in Hydrogen Transfer Reactions, Acc. Chem. Res. 44 (2011) 379–391, https://doi.org/10.1021/ar1001582.

[71] R.F. Perez, O.S.G.P. Soares, A.M.D. de Farias, M.F.R. Pereira, M.A. Fraga, Conversion of hemicellulose-derived pentoses over noble metal supported on 1D multiwalled carbon nanotubes, Appl. Catal. B: Environ. 232 (2018) 101–107, https://doi.org/10.1016/j.apcatb.2018.03.042.

[72] S.L.B.V. Carvalho, E.B. de Moraes Medeiros, A. de Souza Wanderley, L.d. M. Ribeiro, J.G. da Silva, I.T. de Almeida Simões, N.C. do Rego Lemos, N.J. Ribeiro Neto, C.A.M. de Abreu, H.M. Baudel, N.M. de Lima Filho, Production of xylitol from acidic hydrolysates of lignocellulosic biomass by catalytic hydrogenation over a Ni–Ru/C catalyst, Chem. Eng. Res. Des. 174 (2021) 11–18, https://doi.org/10.1016/j.cherd.2021.07.025.